Electrochimica Acta 56 (2011) 7012–7021

Contents lists available at ScienceDirect

Electrochimica Acta

journal homepage: www.elsevier.com/locate/electacta

Voltammetric investigations on the transition between dissolution, passivation and deposition characteristics of Ni, Cu and their alloys in fluorine based ionic liquid

S. Sathyamoorthi [a], D. Velayutham [a], V. Suryanarayanan [a,*], M. Noel [b]

[a] Electroorganic Division, CSIR-Central Electrochemical Research Institute, Karaikudi 630 006, India
[b] School of Chemistry, Karunya University, Coimbatore 641 114, India

ARTICLE INFO

Article history:
Received 17 March 2011
Received in revised form 1 June 2011
Accepted 1 June 2011
Available online 13 June 2011

Keywords:
Anodic behavior
Ni passivity
Monel dissolution
Reversibility
Fluoride salts

ABSTRACT

Multisweep cyclic voltammetric (CV) responses of nickel, copper, Monel and nickel–copper alloy had been extensively studied and compared in a variety of non-aqueous solvents such as acetonitrile (AN), propylene carbonate (PC) and sulfolane containing triethylamine trishydrogen fluoride (TEA·3HF) ionic liquid. The quantity of dissolution as well as surface morphological transformation on the electrode surfaces as a result of anodic polarization were investigated using atomic absorption spectroscopy (AAS) and scanning electron microscopy (SEM) respectively. The nature of crystallites formed on the polarized electrode was characterized using X-ray diffraction (XRD). The voltammetric study clearly indicates that Ni, Monel and Ni–Cu alloy are passive and stable in neat TEA·3HF medium in the recorded potential region of CV. Surface morphology of Ni after polarization, reveals the generation of pits, whereas the evolution of small crystallites of CuF_2 are noted on the polarized alloy material, as evidenced by SEM pictures. Copper electrode shows reversible voltammetric characteristics with high charge recovery ratio (q_c/q_a) suggesting that in this medium, Cu can certainly serve as reference electrode. Addition of water in TEA·3HF medium increases the solubility and stability of these metal fluoride film. In solvents such as PC, AN and sulfolane containing TEA·3HF, Ni and their alloys exhibit remarkable passivity and the charge recovery ratio decreases to some extent for Cu. In TEA·3HF/AN medium, the dissolution of Cu is very high. The present investigation suggests that the relative stability of all the four electrodes in neat TEA·3HF and solvents containing 0.1 M TEA·3HF decreases in the order: Ni > Monel > Ni–Cu alloy > Cu and relative solubility of metal fluoride films in the three solvents increases in the order: PC < sulfolane < AN.

© 2011 Elsevier Ltd. All rights reserved.

1. Introduction

Electrochemical perfluorination is one of the well-established processes for the production of perfluorinated organic compounds in an industrial scale [1]. Literature studies reveal that nickel electrode has been used as the successful anode material not only for this process [2–6] and also for the production of high purity NF_3 in NH_4F containing melts [7–10].

Mechanistic studies [11–13] and reviews [14,15] have clearly brought out the catalytic role of electrogenerated NiF_2 and its high valent fluoride films during the electrochemical fluorination of organic compounds. Two reaction pathways have been already established in which the first one deals with the free radical pathway where the loosely held fluorine-free radical formed on the active films attacks the organic compounds [11–13] and the second one describes the formation of adsorbed organic intermediate on the active fluoride film via the evolution of carbocation mechanism [16,17] leading to the formation of perfluoro products. Hence, it is of paramount importance in studying about the characteristic properties of the NiF_2 film generated as a result of electrochemical dissolution of Ni within the voltammetric potential region of 0.6 V vs H_2.

There are only few reports in the literature focusing their investigation on this electrochemically generated NiF_2 film in this specified potential region. In our laboratory, the effect of addition of CH_3CN and water on the stability and solubility of this NiF_2 film has been studied in Et_3N·3HF medium [18,19]. The investigations reveal that acetonitrile enhances the dissolution of Ni, whereas water induces the Ni dissolution as well as the hydrolysis of NiF_2 film leading to the formation of oxides and oxyfluorides [19]. In recent studies, cyclic voltammetric investigations on the electrochemical fluorination of $(CH_3)_4NF$·4.0HF/Me_3N·3HF containing different percentages of CsF·2.0HF on Ni anode show that the addition of

* Corresponding author. Tel.: +91 4565 227550; fax: +91 4565 227779.
E-mail addresses: vidhyasur@yahoo.co.in, surya@cecri.res.in (V. Suryanarayanan).

0013-4686/$ – see front matter © 2011 Elsevier Ltd. All rights reserved.
doi:10.1016/j.electacta.2011.06.006

CsF·2.3HF (wt% 50) melt suppresses the passivation of the Ni anode and increases the electric conductivity of the NiF_2 film, thereby leading to an increase the current density in the voltammetric potential region higher than 3.5 V vs Ag/Ag^+ [20–22].

Hence, in this work, the stability and solubility of the electrochemically generated surface fluoride film had been studied in three solvent media namely sulfolane, acetonitrile and propylene carbonate. Sulfolane is highly viscous solvent and even, electrochemical perfluorination of this solvent on Ni electrode in AHF medium has been reported in the literature [23,24]. The other two solvents had been selected based on their different polarisable properties. There are three main objectives for this work: What are the influences of the above solvents on the solubility of NiF_2 film? Whether the stability of the NiF_2 film could be enhanced by employing Ni–Cu alloy materials instead of pure Ni? What will the nature of dissolution of electrode material during the addition of trace amount of water in fluoride medium?

In order to answer the above questions, triethylamine trishydrogen fluoride (TEA·3HF) has been taken as fluoride source for the generation of NiF_2 film as this ionic liquid is less corrosive in nature and easy to handle even at room temperature. In addition to Ni, two alloy materials namely Monel (composition of about Ni (wt% 66) and Cu (wt% 31)) and Ni–Cu (consisting of about Cu (wt% 66) and Ni (wt% 30)) were taken as the working electrodes in this work. These alloy electrodes are highly corrosion resistant as evidenced by a literature study where the anodic protection had been provided by evolution of passive NiF_2 film, which is irreducible at potentials less than that of hydrogen evolution [25]. Further, pure Cu electrode was also used for the comparative purpose. The transition from dissolution/passivation behavior of NiF_2 to the redox behavior of Cu/CuF_2 film through the alloy composition is investigated using cyclic voltammetry (CV), scanning electron microscope (SEM), X-ray diffraction (XRD) and atomic absorption spectroscopic (AAS) techniques.

2. Experimental

The ionic liquid, TEA·3HF was prepared by mixing TEA with freshly taken AHF (TANFAC, India) at the temperature range of freezing mixture, evaluating the HF content by titration and adjusting the TEA·3HF ratio accordingly [18]. The working electrodes were Ni, Cu and their alloys (area was $0.2\,cm^{-2}$). Compositions of Monel and Ni–Cu alloy were found out from energy dispersive X-ray spectroscopy (EDX) analysis. The elements found in the Monel and Ni–Cu alloy included: Ni (wt% 66.03) and Cu (wt% 31.22) as well as Ni (wt% 30.36) and Cu (wt% 66.45) respectively in significant amounts, while Fe, Mn, Co, Al, and Si were present only in traces. All the working electrodes except Cu were polished to mirror finish and washed repeatedly with triple distilled water followed by trichloroethylene before use. Since an insoluble film is formed on during each potential cycle, these electrodes had to be repeatedly cleaned and polished after each CV experiment in order to get reproducible results. Preliminary voltammetric experiments employing Cu rod as working electrodes in such fluoride media indicated some difficulties in achieving the reproducibility where very high anodic dissolution was noticed. Hence, fresh Cu foil was used for each experiment.

The choice of reference electrode posed some problems. The palladium (Pd/H_2) electrode showed instability, especially in TEA·3HF in which Pd dissolution was noticed. Hence, a Pt wire was used as a quasi-reference electrode. The measurements suggested that the Pt quasi-reference potential in TEA·3HF was always close to the Pd/H_2 reference electrode within the limit of ±20 to ±30 mV. The reference potential, however, was checked from time to time externally against a saturated calomel electrode (SCE). A Pt foil as counter electrode in a polypropylene undivided cell was used throughout the work.

Acetonitrile (high-performance liquid chromatography grade), propylene carbonate (analytical reagent (AR) grade), sulfolane (AR grade), and triple-distilled water were used as solvents. Voltammetric measurements were carried out using an Autolab PGSTAT302N system under computer control. Scanning electron microscopy (SEM) was performed with JEOL, model 30CF instrument. For the XRD measurement, Xpert PRO PANalytical Philips instrument was used. The amount of Ni^{2+} and Cu^{2+} species dissolved in the electrolyte was estimated using atomic absorption spectroscopy (AAS, GBC 906 AA, and Australia). For the AAS analysis, the working electrodes were anodically polarized in neat TEA·3HF and solvents containing 0.1 M of TEA·3HF at a slow sweep rate of $40\,mV\,s^{-1}$ within the corresponding potential limit (five cycles). After polarization, 0.25 ml of the electrolyte was pipetted out and made up to 10 ml using triple-distilled water, and this diluted portion was subjected for AAS analysis. All the experiments were carried out at 303 ± 1 K.

3. Results and discussion

3.1. CV studies in TEA·3HF

Typical multisweep CVs of Ni, Monel, Ni–Cu alloy and Cu electrodes in neat TEA·3HF medium at a same sweep rate of $40\,mV\,s^{-1}$ are shown in Fig. 1a–d respectively. In general, the potential limits recorded for Ni and its alloys in the CV were approximately between −0.75 V and 0.5 V for Cu, it is −1.0 V to 0.5 V unless otherwise specified. Different voltammetric parameters such as anodic and cathodic peak potentials (E_{pa} and E_{pc}), anodic and cathodic charge densities (q_a and q_c) as well as charge recovery ratio (q_c/q_a) obtained from the CVs are indicated in Table 1. Nickel exhibits a well defined anodic peak at −0.1 V vs. Pt in the forward sweep, and there is no cathodic reduction peak in the reverse sweep. The irreversible process is associated with two well known electrochemical reactions namely the dissolution of Ni to Ni^{2+} followed by the formation of passive NiF_2 film [16]. In all subsequent sweeps, complete passivation of Ni is noted in this medium (Fig. 1a).

Monel (Fig. 1b) and Ni–Cu alloy (Fig. 1c) electrodes retain the passivity and irreversibility, a similar behavior exhibited by Ni, to a greater extent. Both the electrodes get oxidized approximately at the same potential region of 0.1 V (Table 1) and on the reverse sweep, cathodic currents are not observed at the passivated electrode surface; thus the passive film on both these alloys consists in parts of Ni fluoride film, which is irreducible at potentials less negative than that for hydrogen evolution and this film appears to prevent dissolution of Cu as well. In fact, two anodic oxidation peaks are observed on the Monel (Fig. 1b) and this may be associated with two overall stages of oxidation (say NiF_2 and then CuF_2 formation or two distinct phases (outer phase or inner phase)). The anodic dissolution charge density for Ni–Cu alloy is three fold higher than that of Ni and Monel electrodes (Table 1).

Voltammograms of copper show well defined reversible behavior in TEA·3HF medium, where a single anodic peak at around 0.1 V followed by two cathodic peaks at around −0.44 and −0.63 V are noted and the peak currents do not vary significantly during second and subsequent sweeps (Fig. 1d and Table 1). The charge recovery ratio (q_a/q_c) for Cu in this medium is around 0.88 suggesting that during each redox cycle (five cycles), around 12% of dissolved copper remains in solution without undergoing redepostion during the cathodic sweep. The perfect reversibility and the high charge recovery ratio imply that, in this medium, Cu can indeed serve as reference electrode [26]. Overall, it is important to note that the

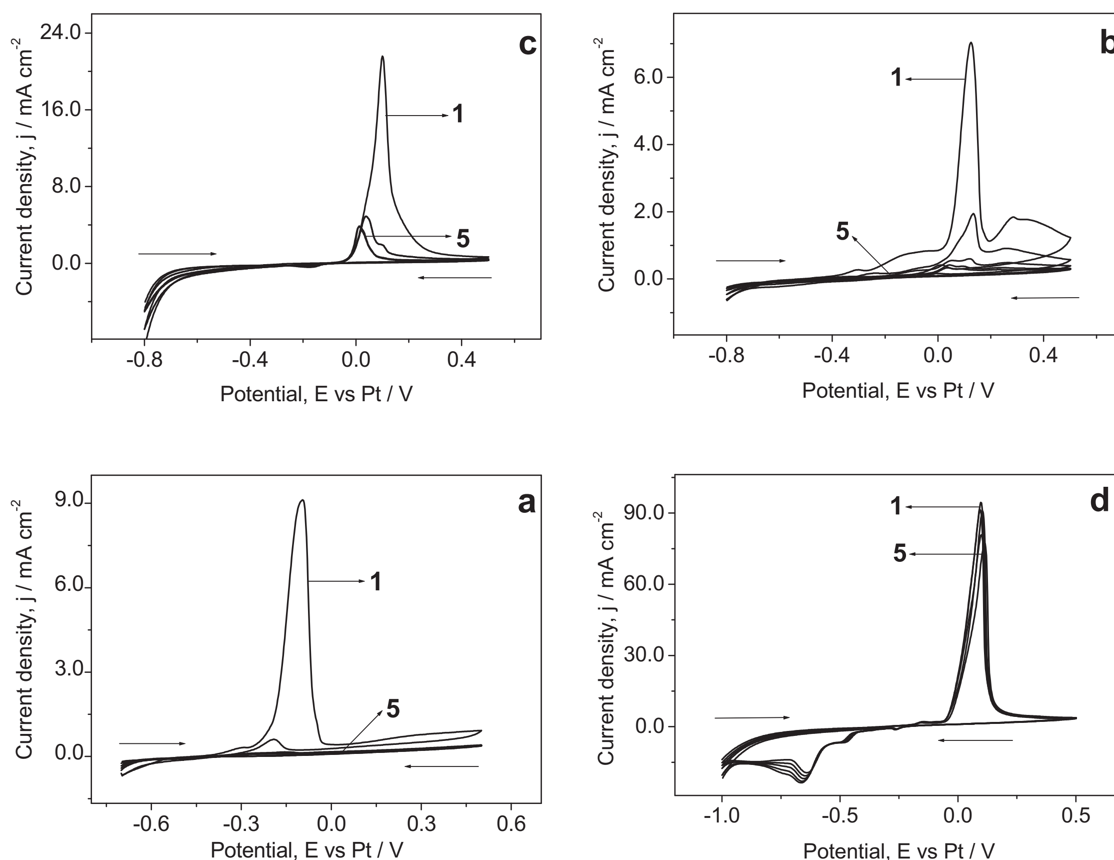

Fig. 1. Multisweep cyclic voltammograms of (a) Ni, (b) Monel, (c) Ni–Cu alloy and (d) Cu in neat TEA·3HF at a sweep rate of 40 mV s^{-1}. Number of cycles = 5.

anodic dissolution charge density increases with the increase of Cu content, which is in the order: Ni < Monel < Ni–Cu alloy < Cu.

Addition of water in TEA·3HF medium influences the voltammetric characteristics of Ni, Cu and its alloys significantly. The multisweep voltammograms suggest that in the presence of 10% water, the main anodic peak shifts 100 mV more positively for Ni (Fig. 2a). The anodic dissolution current and charge increase density substantially with the addition of water, suggesting enhanced Ni dissolution (Table 1). On the contrary, the voltammetric behavior of Monel and Cu–Ni alloy electrodes changes drastically where

Table 1
Voltammetric characteristics of Ni, Cu and their alloys in the absence and presence of solvents containing TEA·3HF at a sweep rate of 40 mV s^{-1}. The standard deviation of the q values is ±2%.

Medium	Electrode	E_{pa} (V)	E_{pc} (V)	q_a (mC cm^{-2})	q_c (mC cm^{-2})	q_c/q_a
TEA·3HF	Ni	−0.10	–	13.5	–	–
	Monel	0.13	–	15.0	–	–
	Ni–Cu alloy	0.10	–	53.0	–	–
	Cu	0.11	−0.63	201.0	176.0	0.88
TEA·3HF/water (wt% 10)	Ni	−0.01	–	105.0	–	–
	Monel	0.13	–	148.0	21.0	0.14
	Ni–Cu alloy	0.14	−0.38	295.0	124.0	0.42
	Cu	0.40	−0.53	619.0	428.0	0.69
TEA·3HF/water (wt% 20)	Ni	0.06	–	576.0	–	–
	Monel	0.11	−0.41	617.0	192.0	0.31
	Ni–Cu alloy	0.33	−0.77	778.0	329.0	0.42
	Cu	0.34	−0.72	906.0	754.0	0.75
TEA·3HF/AN[a]	Ni	−0.32	–	0.1	–	–
	Monel	−0.18	–	3.8	–	–
	Ni–Cu alloy	−0.30	–	4.3	–	–
	Cu	High dissolution				
TEA·3HF/sulfolane[a]	Ni	0.09	–	0.9	–	–
	Monel	0.09	–	1.4	–	–
	Ni–Cu alloy	0.09	–	2.8	1.2	0.41
	Cu	0.23	−0.48	45.0	20.0	0.45
TEA·3HF/PC[a]	Ni	−0.09	–	0.2	–	–
	Monel	−0.04	–	1.2	–	–
	Ni–Cu alloy	−0.01	−0.42	2.8	1.0	0.35
	Cu	0.21	−0.75	27.0	15.0	0.55

[a] Concentration is 0.1 mol dm^{-3}.

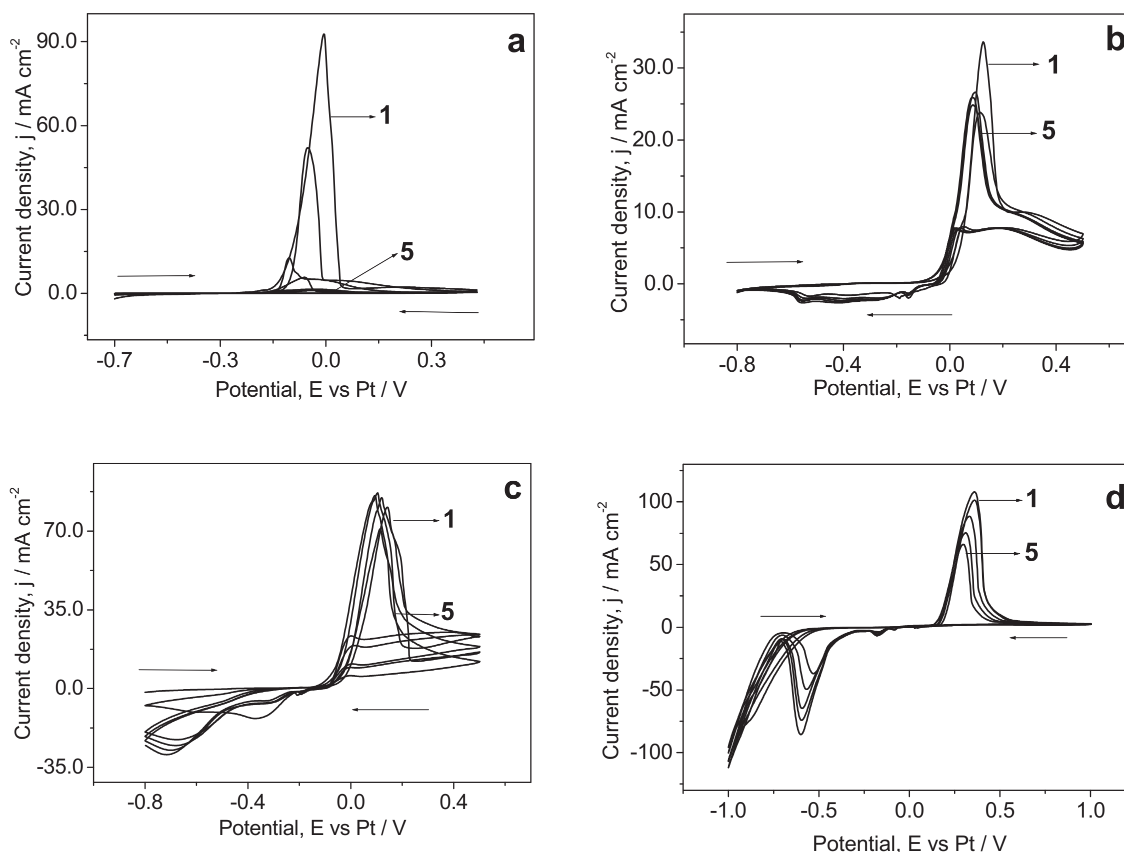

Fig. 2. Multisweep cyclic voltammograms of (a) Ni, (b) Monel, (c) Ni–Cu alloy and (d) Cu in TEA·3HF containing water (wt% 10) at a sweep rate of 40 mV s^{-1}. Conditions are same as in Fig. 1.

the passivity and irreversibility breaks down by the addition of water in the fluoride medium (Fig. 2b and c). The anodic dissolution is initiated at the same potential region, as noted in the neat TEA·3HF, followed by the evolution of cathodic reduction peak in the reverse scan. Higher anodic dissolution charge density than that of neat TEA·3HF is observed for both the electrodes (Table 1). Charge recovery ratio improves with the increase of Cu content. For Cu electrode, the anodic peak shifts towards 300 mV in the positive direction and the q_c/q_a value for Cu also decreases considerably when compared to neat TEA·3HF medium. Once again, the anodic dissolution increases from pure Ni to Ni–Cu alloy and Cu. With the further addition of water (20%), the values of anodic peak potential remain almost unaltered for Ni and Monel, however, a slight increase towards positive value is noted for Ni–Cu alloy. Others wise, similar dissolution pattern is noticed for all the four electrodes.

3.2. CV studies in solvents containing TEA·3HF

Typical multi-sweep CVs of Ni, Monel and Ni–Cu alloy in acetonitrile containing 0.1 M of TEA·3HF medium at the same sweep rate of 40 mV s^{-1} are shown in Fig. 3a–c respectively. The anodic peak for Ni electrode in this medium appears at −0.32 V, and this is a negative shift when compared to the peak potential noted in neat TEA·3HF medium. Further, the anodic peak decreases initially and then increases linearly with the applied positive potential. This phenomenon may be associated with the growth of NiF_2 layer. Further, the passivity remains the same, as found out with very low current in the second and subsequent sweeps (Fig. 3a). The dissolution charge density becomes very low in this medium (Table 1).

Distinct anodic peaks are noted for Monel and Ni–Cu alloy in AN containing 0.1 M TEA·3HF medium, where the dissolution–passivation process is completed below 0.0 V (Fig. 3b and c). The anodic dissolution charge density, q_a increases slightly with the increase of the Cu content (Table 1). On the other hand, high anodic dissolution is noted for Cu in 0.1 M TEA·3HF/AN medium where getting reproducible voltammograms becomes a difficult task. As a result of this, no voltammograms were recorded for Cu in this medium. From the above studies, it may be concluded that, in this medium, on both the alloys, NiF_2 film plays an important role in controlling the drastic dissolution of Cu.

The voltammograms of Ni and its alloys recorded in PC and sulfolane containing 0.1 M TEA·3HF medium show good passivity. The anodic peak potential is evolved at 0.09 V in sulfolane (Fig. 4a–c) and it shifts towards the cathodic direction in PC containing fluoride medium (Fig. 5a–c). The total anodic dissolution charge density does not exceed 3 mC cm^{-2} (Table 1). For Cu electrode, the reversibility is still maintained (Figs. 4d and 5d); however the dissolved copper is not getting deposited efficiently during the reverse sweep as noted from the charge recovery ratio of 55% or less. The overall anodic dissolution charges densities are lower than that of neat TEA·3HF (around 45 mC cm^{-2} for sulfolane and 27.0 mC cm^{-2} for PC containing fluoride medium) (Table 1).

The overall dissolution/passivation/deposition behaviors of all the four electrodes in five different media are compared in Fig. 6 using their q_a and q_c values, obtained from the CV. Nickel and its alloys are relatively stable in neat TEA·3HF and the solvents containing TEA·3HF, as noted from their lower q_a values than that of Cu (Fig. 6a, c, d and e). Presence of water in the neat ionic liquid increases the anodic dissolution of all the electrodes significantly (Fig. 6b).

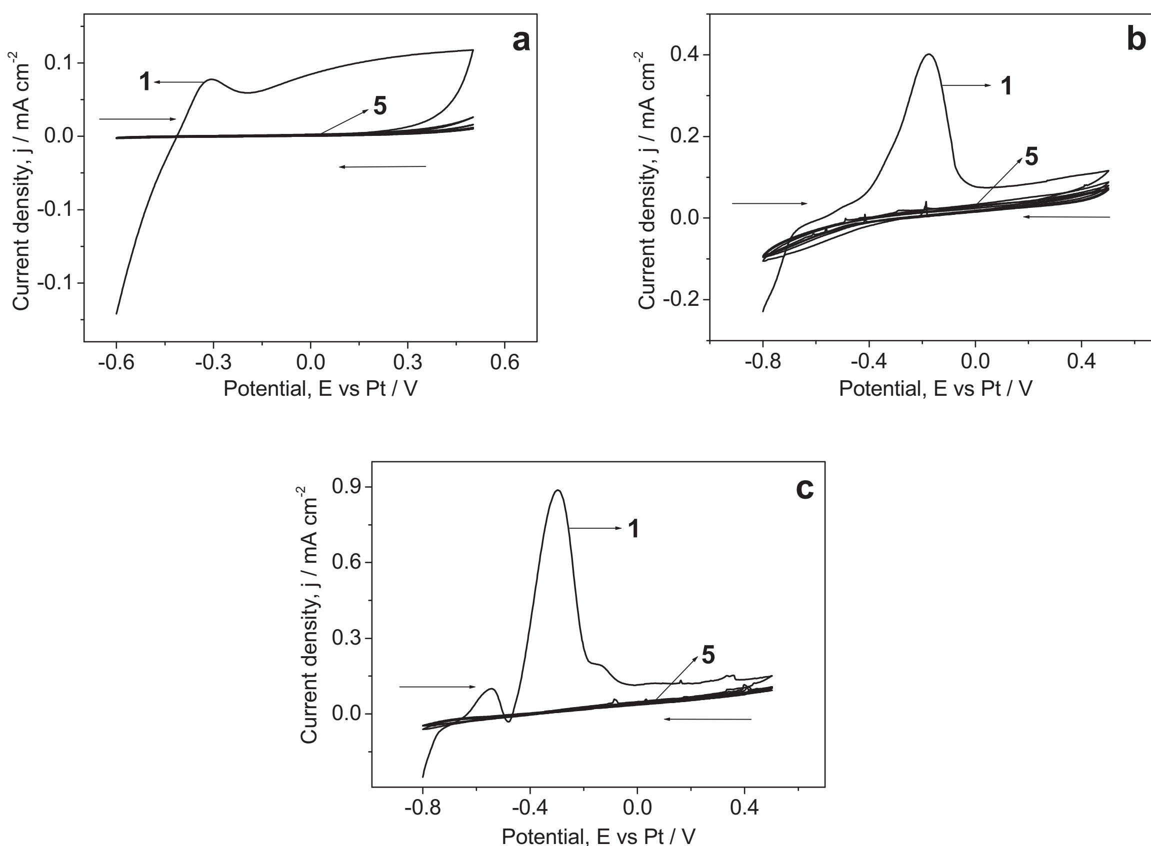

Fig. 3. Multisweep cyclic voltammograms of (a) Ni, (b) Monel and (c) Ni–Cu alloy in acetonitrile containing 0.1 M TEA·3HF at a sweep rate of 40 mV s^{-1}. Conditions are same as in Fig. 1.

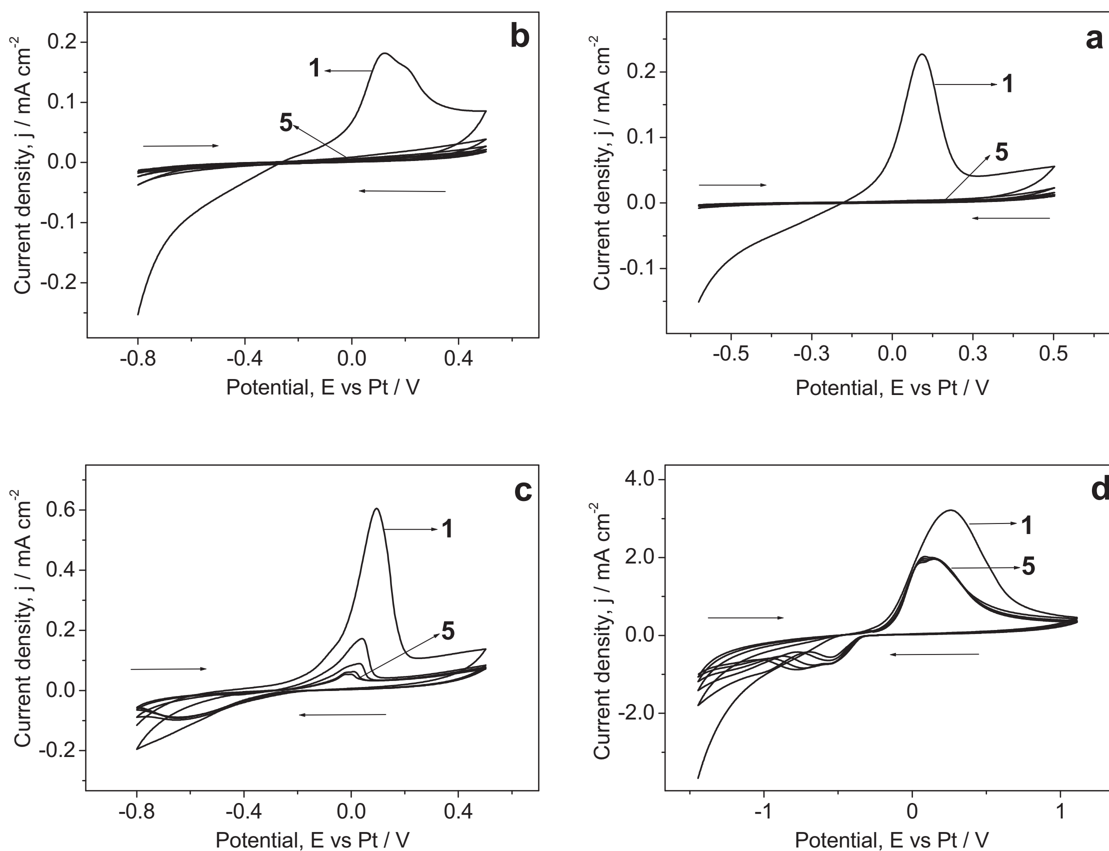

Fig. 4. Multisweep cyclic voltammograms of (a) Ni, (b) Monel, (c) Ni–Cu alloy and (d) Cu in sulfolane containing 0.1 M TEA·3HF at a sweep rate of 40 mV s^{-1}. Conditions are same as in Fig. 1.

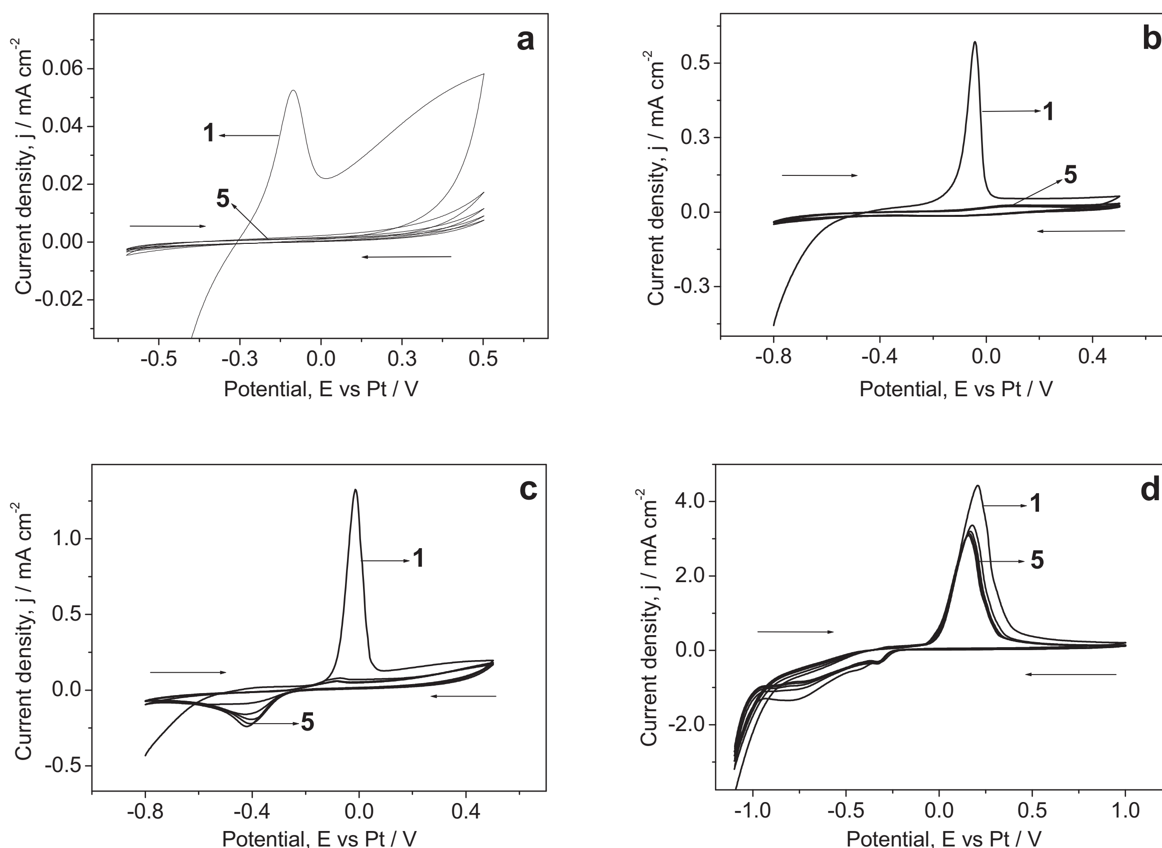

Fig. 5. Multisweep cyclic voltammograms of (a) Ni, (b) Monel, (c) Ni–Cu alloy and (d) Cu in PC containing 0.1 M TEA·3HF at a sweep rate of 40 mV s^{-1}. Conditions are same as in Fig. 1.

Copper fluoride is relatively more soluble in all electrolyte systems investigated in this work. In the neat ionic liquid containing high fluoride ion concentration, both the dissolution (q_a) and precipitation (q_c) is significantly high with a good charge recovery ratio (Fig. 6a). In PC and sulfolane containing TEA·3HF media, at least 50% of charge recovery ratio is maintained, though both the q_a and q_c become low (Fig. 6d and e). It is important to mention here that the potential window taken in recording the CVs for Cu is wider than that of other electrodes in all the media and as a result of this, both the anodic and cathodic dissolution charge densities of Cu are also high. The overall anodic dissolution of all the electrodes in TEA·3HF and different solvents containing TEA·3HF decreases in the order: TEA·3HF > TEA·3HF/AN > TEA·3HF/sulfolane > TEA·3HF/PC.

3.3. Surface characterization by SEM

Images of SEM obtained for Ni, after potentiostatic polarisation at 0.0 V for 15 min, Monel, Ni–Cu alloy and Cu electrodes, after potential cycling (six cycles) in neat TEA·3HF medium, are shown in Fig. 7a–d respectively. Appearance of circular pits over the compact passive NiF_2 layer (Fig. 7a) ensures the Ni passivation in the passive potential region of 0.0 V, confirming the earlier result [18].

With the addition of Cu to Ni (31.22% of Cu corresponding to Monel), the pitting pattern completely disappears and the evolution of small crystallites of CuF_2 is noted as a result of the Cu dissolution and CuF_2 precipitation along with NiF_2 crystallites (Fig. 7b). Further increase of Cu (66.45% of Cu in Ni–Cu alloy) leads to an increase in the number of CuF_2 crystallites (Fig. 7c). The SEM image of copper shows that after the anodic polarization of Cu in TEA·3HF results in the formation of a uniform porous CuF_2 layer, on which the precipitated Cu crystallites are located (Fig. 7d). The uniform base CuF_2 layer probably ensures better charge recovery ratio during potential cycling.

Addition of water to neat TEA·3HF brings about substantial morphological changes on the fluoride film formed as a result of potentiostatic and cyclic polarization. In the pre-passive region, water enhances the solubility of NiF_2 film leading to a decrease of the depth of the pits (compare Figs. 7a and 8a). The above results show that the water enhances uniform dissolution/passivation process on Ni during the anodic polarization. In the Monel electrode, the CuF_2 dissolves completely thus exposing the heterogeneous NiF_2 crystallites on the surface (Fig. 8b). With high Cu content in the Ni–Cu alloy, the re-precipitated CuF_2 particles are formed on the surface indicating the instability of the film (Fig. 8c). The SEM pictures of Cu electrode, obtained after the polarization in water as and in acetonitrile containing fluoride media, are found to be featureless as the electrode undergoes severe dissolution in the above two media. Hence, the corresponding morphological pictures are not shown here.

All the four electrodes exhibit remarkable stability in sulfolane and PC containing 0.1 M TEA·3HF medium. Typical SEM pictures of all the electrodes obtained in sulfolane medium alone are presented in Fig. 9. Even under anodic polarization in the prepassive region, Ni exhibits uniform film formation (Fig. 9a). The pits observed on surface of all the four electrodes are small and uniformly distributed (Fig. 9a–d).

3.4. Film characterization by XRD

In order to identify the nature of crystalline face formed on the surface of the electrodes, XRD analysis of the polarized electrode was carried out. Though the polarization was done for 2 h, the obtained fluoride films were very thin and hence the XRD sig-

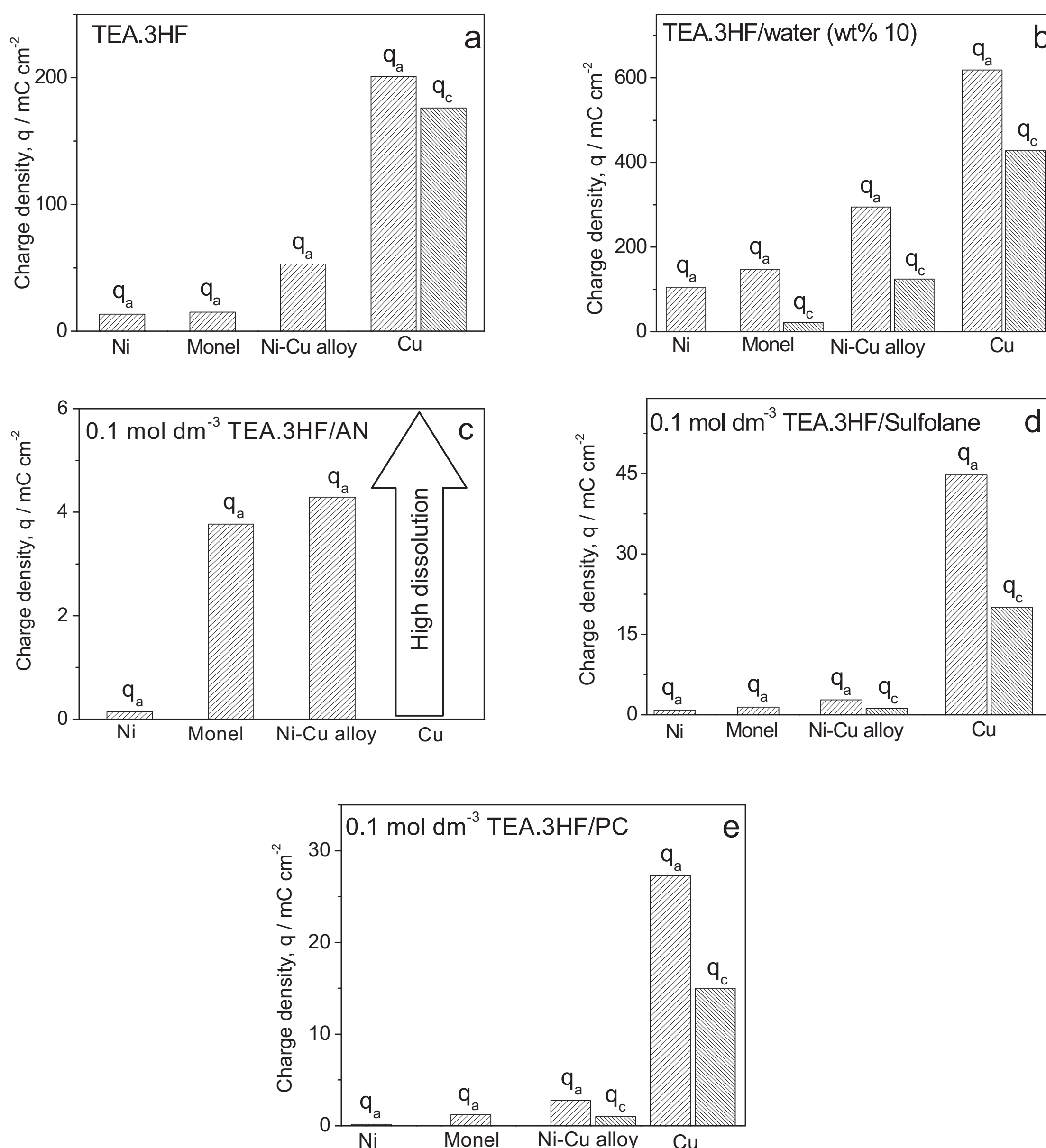

Fig. 6. Effect of anodic and cathodic charge densities on the cyclic polarization of Ni, Monel, Ni–Cu alloy and Cu in (a) neat TEA·3HF, (b) TEA·3HF/water (wt% 10) and 0.1 M TEA·3HF in (c) AN, (d) sulfolane and (e) PC.

nals were also weak. Further, no characteristics XRD signals were noticed for the electrodes polarized in solvents containing 0.1 M TEA·3HF and this may be correlated with comparatively lower q_a values than that of neat TEA·3HF system. Table 2 shows the XRD characteristics of fluoride films formed on all the four electrodes after polarization in neat TEA·3HF and TEA·3HF containing water (wt% 10). On Ni and Monel electrodes, $NiF_2 \cdot 4H_2O$ was identified as crystalline phase and $CuF_2 \cdot 2H_2O$ was found to be predominant phase on Ni–Cu alloy as well as on Cu electrode. The above results reveal that the fluoride film of predominant metal in the alloy dominates over the other.

The anodic oxidation peak for Cu as well as Ni occurs in a narrow potential region. The actual metal dissolution may also occur due to the mixed potential process at crystal defects. Hence the percentage

Table 2
XRD features of Ni, Cu and their alloys after anodic polarization in neat TEA·3HF and TEA·3HF/water (wt% 10).

Medium	Electrode	*d*-value (Å)	Intensity (%)	Characterized material
TEA·3HF	Ni	4.798	1.03	$NiF_2 \cdot 4H_2O$
	Monel	4.846	5.37	$NiF_2 \cdot 4H_2O$
	Ni–Cu alloy	4.731	3.13	$CuF_2 \cdot 2H_2O$
	Cu	4.731	8.43	$CuF_2 \cdot 2H_2O$
TEA·3HF/water (wt% 10)	Ni	4.853	0.41	$NiF_2 \cdot 4H_2O$
	Monel	4.852	4.25	$NiF_2 \cdot 4H_2O$
	Ni–Cu alloy	4.729	8.64	$CuF_2 \cdot 2H_2O$
	Cu	4.724	7.16	$CuF_2 \cdot 2H_2O$

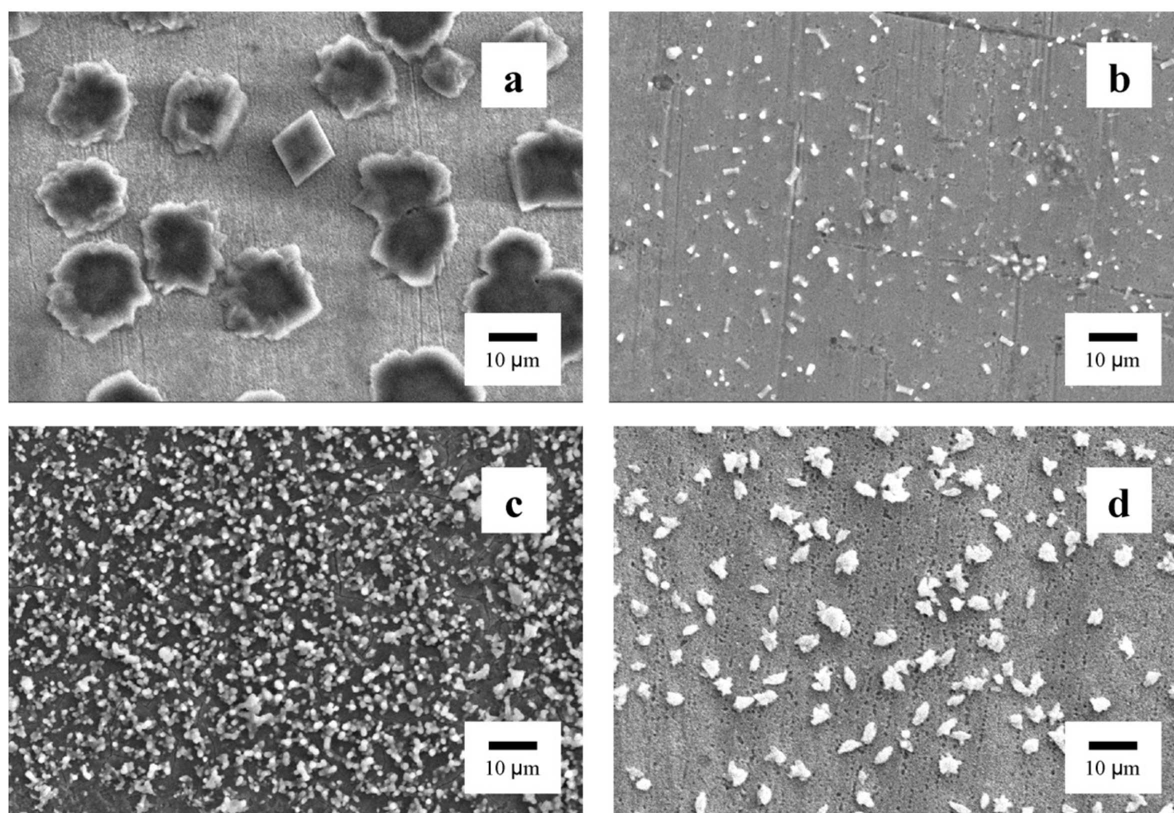

Fig. 7. SEM images of (a) Ni (polarized for 15 min at 0 V), (b) Monel, (c) Ni–Cu alloy and (d) Cu (polarized up to 6 cycles) in neat TEA·3HF at 40 mV s^{-1}. Magnification (a–d, 1k×).

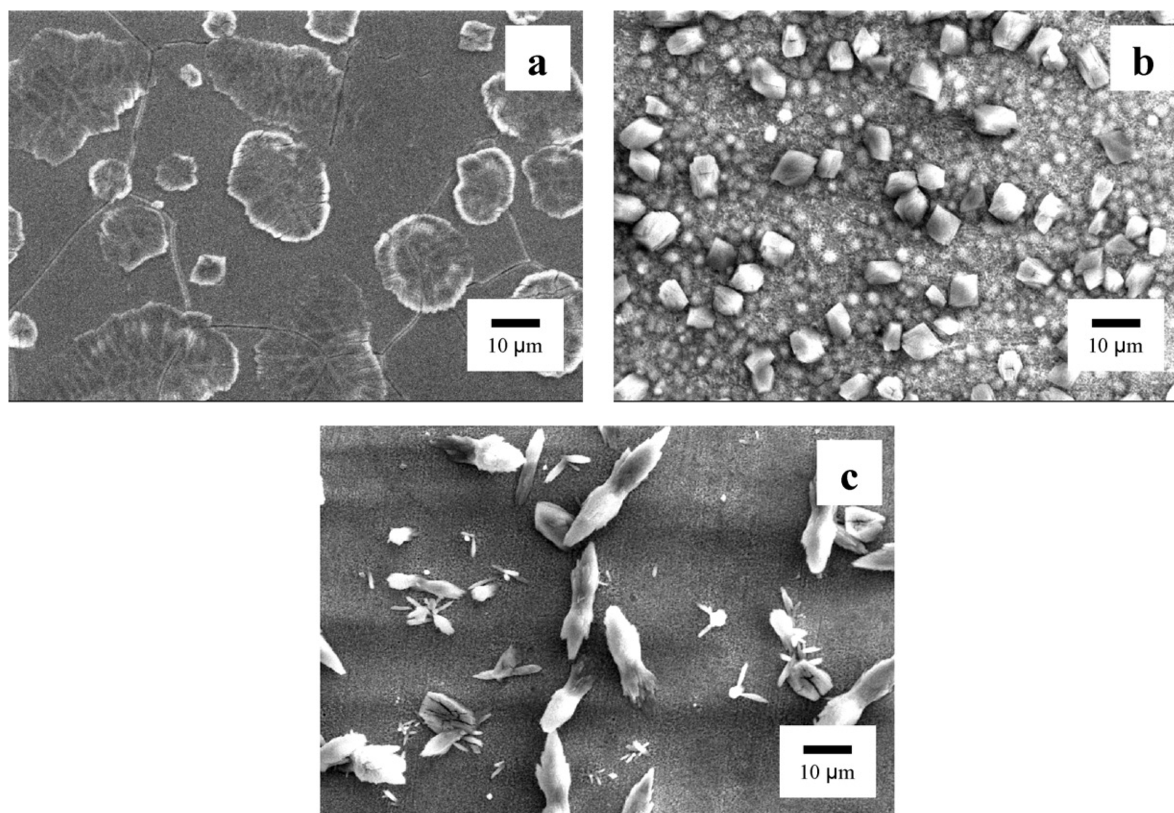

Fig. 8. SEM images of (a) Ni (polarized 15 min at 0.1 V), (b) Monel and (c) Ni–Cu alloy in TEA·3HF/water (wt% 10) at 40 mV s^{-1}. Magnification (a–d, 1k×). Other conditions are same as in Fig. 7.

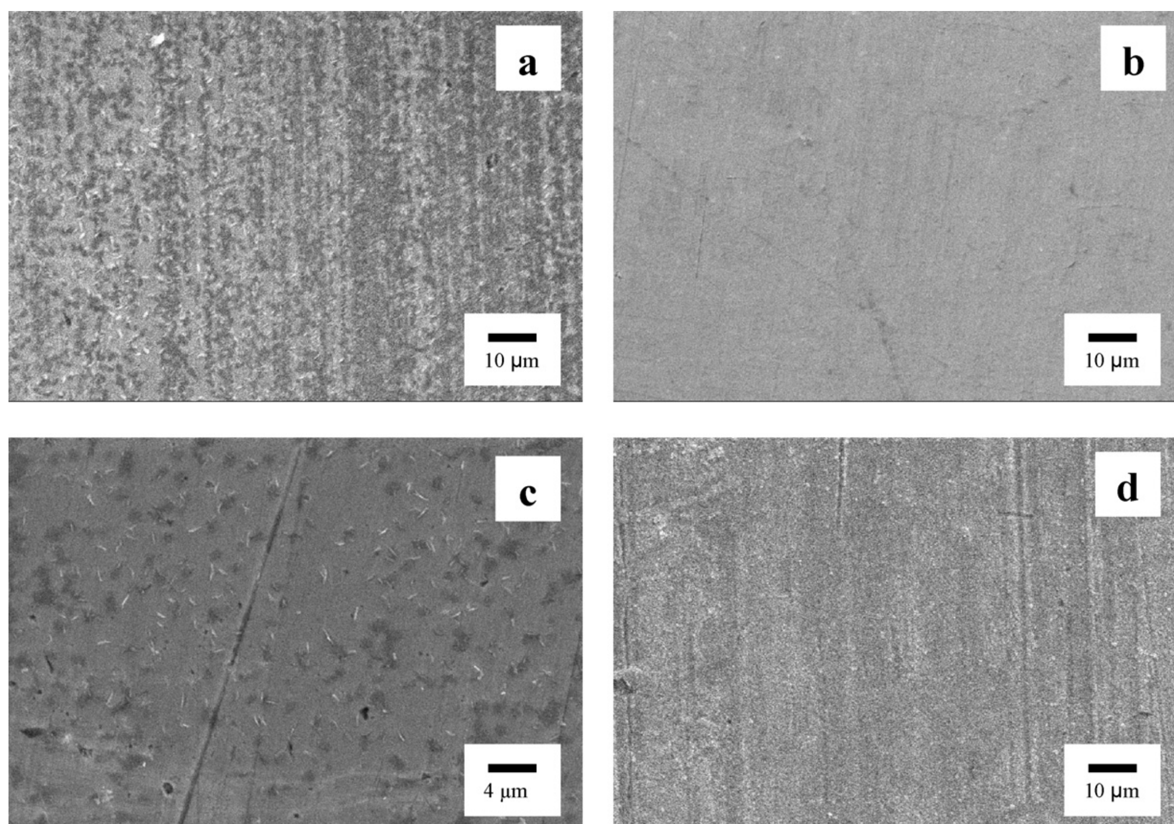

Fig. 9. SEM images of (a) Ni (polarized 15 min at 0.25 V), (b) Monel, (c) Ni–Cu alloy and (d) Cu in sulfolane containing 0.1 M TEA·3HF at 40 mV s^{-1}. Magnifications (a, b and d 1k×, c 2k×). Other conditions are same as in Fig. 7.

of dissolution of individual metallic species after the voltammetric cycling was further analyzed by AAS of the electrolyte solution.

3.5. Metal dissolution analysis by AAS

The AAS analysis also provides some interesting insights on the relationship between dissolution charge density and quantity of metal ions dissolved in the electrolyte. In neat TEA·3HF medium, no Ni^{2+} species was detected in the electrolyte solution, whereas in Monel and Ni–Cu alloy, substantial quantity of metal ions were present. This clearly indicates the breakdown of passivity of heterogeneous surface of alloy material, where one metal initiates the dissolution of the other one (Table 3). Cu electrode in this medium, even though, shows high anodic dissolution charge density, the quantity of Cu^{2+} in the analyte is found to be comparable with the amount of copper ions in the solution where Ni–Cu alloy had been polarized. The above result shows that deposition of Cu^{2+} to Cu is highly feasible (compare q_c and q_a values in Table 1) leading to good charge recovery ratio.

Once again, the presence of water in TEA·3HF increases metal dissolution, as noted from the linearity between the quantity of metal ions present and anodic dissolution charge density (Table 3). Hence, AAS data reveals the presence of large quantities of both Ni^{2+} and Cu^{2+} ions in the solution. It is important to note that the quantity of Cu^{2+} obtained from the anodic dissolution of Monel is found to be higher than that of Ni–Cu alloy, though the percentage of Cu in Monel is naturally found to be lesser that of Ni–Cu alloy. This phenomenon may be correlated with lesser q_c/q_a value obtained for Monel when compared to Ni–Cu alloy, wherein only a small part of the dissolved Cu^{2+} may be deposited as Cu and as a result of this, major metal ions remain only in solution. For pure Cu, once again, q_c/q_a decreases substantially with the addition of water.

Once again, in sulfolane containing TEA·3HF medium, no Ni was detected (Table 1). With the addition of Cu, the dissolution of Ni gets started and in Ni–Cu alloy, it decreased slightly (Table 3). No

Table 3
AAS data for the dissolved metallic species obtained after the anodic polarization of Nickel, Cu and their alloys in different fluoride media.

Medium	Electrode	Ni (×10^{-9} mol dm^{-3})	Cu (×10^{-9} mol dm^{-3})
TEA·3HF	Ni	–	Nil
	Monel	433	44
	Ni–Cu alloy	380	76
	Cu	Nil	92
TEA·3HF/water (wt% 10)	Ni	1361	Nil
	Monel	5411	1191
	Ni–Cu alloy	784	285
	Cu	High dissolution	
0.1 mol dm^{-3} TEA·3HF/sulfolane	Ni	–	Nil
	Monel	67	22
	Ni–Cu alloy	49	17
	Cu	Nil	32

AAS analysis was carried for Cu in 0.1 M TEA·3HF/AN because of its severe dissolution in this medium. Otherwise, similar trend in the dissolution behavior is followed for all the electrodes polarized in AN and PC containing TEA·3HF medium.

From the above studies, it is understandable that q_a value for Ni is correlated with its dissolution process, whereas for Cu, the former corresponds to the relative solubility of fluoride salts and q_c belongs with the film thickness as well as its coverage on the electrode surface in addition to the deposition of Cu^{2+} ions. The above results show that the relative stability of all the four electrodes in neat TEA·3HF and solvents containing TEA·3HF media decreases in the order: Ni > Monel > Ni–Cu alloy > Cu and relative solubility of metal fluoride films in the three solvents increases in the order: PC < sulfolane < AN.

4. Conclusions

The present voltammetric study clearly indicates that Ni is quite stable in neat TEA·3HF medium in the passive-potential region. The film dissolution occurs through pit generation in the active/passive region as noted from the SEM pictures. The Monel and Ni–Cu alloy retain the passivity and irreversibility, a similar behavior exhibited by Ni, to a greater extent. However, the SEM morphology of polarized electrodes in this medium show that the pitting pattern completely disappears and the evolution of small crystallites of CuF_2 are noted as a result of the Cu dissolution and CuF_2 precipitation. The voltammetric results confirm the prevention of further dissolution of Cu by the formation of compact thin film of NiF_2 over the Cu surface in both these alloys.

On the other hand, the copper electrode shows reversible voltammetric characteristics with high charge recovery ratio (q_c/q_a) suggesting that in this medium, Cu can certainly serve as reference electrode. Addition of water in TEA·3HF influences high anodic dissolution of all these electrodes, as confirmed from SEM pictures. In solvents such as PC, AN and sulfolane containing TEA·3HF, Ni exhibits remarkable passivity and stability and with the addition of Cu, the dissolution of Ni gets induced, as confirmed by AAS analysis. The percentage of reversibility decreases for Cu in PC and sulfolane containing the fluoride media and in TEA·3HF/AN medium, severe dissolution is noted.

On Ni and Monel electrodes, $NiF_2{\cdot}4H_2O$ was the identified as crystalline phase, whereas $CuF_2{\cdot}2H_2O$ was found to be predominant phase on Ni–Cu alloy and Cu electrode, as found out from XRD analysis. The above studies reveal that the relative stability of the four electrodes in neat TEA·3HF and solvents containing 0.1 M TEA·3HF media decreases in the order: Ni > Monel > Ni–Cu alloy > Cu and relative solubility of metal fluoride films in the three solvents increases in the order: PC < sulfolane < AN.

Acknowledgements

The authors thank Director, CSIR-CECRI, Karaikudi for his keen encouragement in publishing this work. Financial support from DST, New Delhi (SR/S1/PC/62/2008) is greatly acknowledged.

References

[1] Y.W. Alsmeyer, W.V. Childs, R.M. Flynn, G.G.I. Moore, J.C. Smeltzer, Organic Fluorine Chemistry: Principles and commercial Applications, Plenum, New York, 1994.
[2] W.V. Childs, L. Christensen, F.W. Klink, C.F. Koplin, H. Lund, M.M. Baizer, Organic Electrochemistry, 3rd ed., Marcel Dekker, New York, 1991.
[3] A.G. Doughty, M. Fleischmann, D. Pletcher, J. Electroanal. Chem. 51 (1974) 456.
[4] J.S. Clarke, A.T. Kuhn, J. Electroanal. Chem. 85 (1997) 299.
[5] N. Watanabe, M. Hrauta, Electrochim. Acta 25 (1980) 461.
[6] T.M. Rangarajan, S. Sathyamoorthi, D. Velayutham, M. Noel, R.P. Singh, R. Brahma, J. Fluorine Chem. 132 (2011) 107.
[7] A. Tasaka, K. Miki, T. Ohasui, S.I. Yamaguchi, M. Kanemaru, N. Iwanaga, N. Aritusuka, J. Electrochem. Soc. 141 (1994) 1460.
[8] A. Tasaka, Y. Tusukda, T. Ohashi, S. Yamada, K. Matasuhita, A. Kohmura, N. Muramatsu, H. Takebayshi, T. Mimaki, Denki Kagaku 65 (1997) 1086.
[9] A. Tasaka, K. Tomoo, A. Takuwa, M. Yamanaka, J. Electrochem. Soc. 145 (1998) 1160.
[10] A. Tasaka, Y. Tusukda, S. Yamada, K. Matsuhjta, A. Kohmura, N. Muramatsu, Electrochim. Acta 44 (1999) 1761.
[11] A. Dimitrov, S. Rudiger, K. Seppelt, T. Peplinski, J. Fluorine Chem. 69 (1994) 15.
[12] S. Rodiger, A. Dimitrov, K. Hottman, J. Fluorine Chem. 76 (1996) 155.
[13] P. Sartori, N. Ignat'ev, S. Datsenko, J. Fluorine Chem. 75 (1995) 157.
[14] P. Sartori, N. Ignat'ev, J. Fluorine Chem. 87 (1998) 157.
[15] F.G. Drakesmith, Topics in Current Chemistry: Electro Fluorination of Organic Compounds, Springer, Berlin, 1997.
[16] B. Zemva, K. Lutar, L. Chacon, M. Fele-Beuermann, J. Allman, C. Shen, N. Bartlett, J. Am. Chem. Soc. 117 (1995) 10025.
[17] N. Bartlett, R.D. Chambers, A.J. Roche, R.C.H. Spink, L. Chacon, J.M. Whalen, J. Chem. Soc. Chem. Commun. (1996) 1049.
[18] M. Noel, N. Suryanarayanan, V. Suryanarayanan, J. Solid State Electrochem. 5 (2001) 419.
[19] M. Noel, V. Suryanarayanan, S. Krishnamoorthy, J. Fluorine Chem. 74 (1995) 241.
[20] Y. Shodai, M. Inaba, K. Momota, T. Kimura, A. Tasaka, Electrochim. Acta 49 (2004) 2131.
[21] A. Tasaka, T. Yachi, T. Makino, K. Hamano, T. Kimura, K. Momota, J. Fluorine Chem. 97 (1999) 253.
[22] A. Tasaka, K. Nakanishi, N. Masuda, T. Nakai, K. Ikeda, K. Momota, M. Saito, M. Inaba, Electrochim. Acta 56 (2011) 4335.
[23] I.N. Rozhkov, A.V. Bukhtiarov, L. Knunyants, Izv. Akad. Nauk. SSSR, Ser. Chem. 4 (1969) 945.
[24] A. Bulan, J. Herzig, US Patent: US 6752917 B2 (2004).
[25] S.Y. Qian, H. Dumont, B.E. Conway, J. Appl. Electrochem. 27 (1997) 1245.
[26] V. Suryanarayanan, M. Noel, J. Solid State Electrochem. 13 (2009) 1913.